



33

34 1. Introduction

35 Predicting the future of the Himalayan cryosphere and water resources depends on understanding the
36 impact of climate change on glaciers (Lutz et al., 2014). About 14–18% of the total glacierized area in
37 Himalaya is debris covered (Kääb et al., 2012). This ratio increases to between 25 and 36% in the
38 Everest region of Nepal (Nuimura et al., 2012; Shea et al., 2015; Thakuri et al., 2014). However, the
39 role played by debris on the surface mass balance of glaciers and, in turn, on the glacier response to
40 climate change remains unclear (Kääb et al., 2012). Indeed, this debris layer insulates the glacier
41 surface from atmosphere when it reaches a sufficient thickness and complicates the response to
42 climate change compared to glaciers with clean ice (Jouvet et al., 2011; Kirkbride and Deline, 2013;
43 Østrem, 1959; Pellicciotti et al., 2015).

44 In comparison with debris-free (clean) ice, melt is enhanced when the surface is covered very thin layer
45 of debris (1–2 cm) as a result of increased absorption of solar radiation and related heat transfer. On
46 the other hand, debris layers thicker than a few centimeters reduce ice melt rates as less surface heat
47 will be conducted through the debris layer and transferred to the ice (Østrem, 1959; Nakawo and
48 Young, 1981; Mattson, 1993; Kayastha et al., 2000; Mihalcea et al., 2006; Nicholson and Benn, 2006;
49 Reid and Brock, 2010; Lambrecht et al., 2011; Lejeune et al., 2013; Brock et al., 2010). However, several
50 studies, based on remote sensing data, have shown comparable rates of elevation changes on debris-
51 covered and clean ice glaciers at similar altitudes in the Himalaya and Karakoram (Gardelle et al., 2013;
52 Kääb et al., 2012). Some studies hypothesized that increased ice cliff ablation and englacial melt on
53 debris covered glaciers could explain these comparable rates of elevation changes (Buri et al., 2015;
54 Immerzeel et al., 2014; Inoue and Yoshida, 1980; Miles et al., 2015). Yet (Ragettli et al., 2015) observed
55 different thinning rates at similar elevations of clean versus debris-covered glaciers in Langtang region
56 (Nepal) using remote sensing techniques. This question of area-averaged melting rates over debris-
57 covered or clean glacier ablation areas remains unanswered.

58 To add complexity, the surface area of debris covered tongues has increased in recent decades due to
59 glacier surface lowering and unstable adjacent slopes, processes that are likely associated with climate
60 change (Bhambri et al., 2011; Bolch et al., 2008; Schmidt and Nüsser, 2009; Shukla et al., 2009).
61 Between 1962 and 2011, the proportion of Everest region glaciers covered by rock debris increased by
62 $17.6 \pm 3.1\%$ (Thakuri et al., 2014) and this proportion could further increase in the future (Rowan et
63 al., 2015).

64 For these reasons, it is urgent to determine the mass balance sensitivity of debris covered glaciers to
65 climate change. Unfortunately, there are very few surface mass balance measurements which have
66 been carried out on debris-covered glaciers (Mihalcea et al., 2006). First, the surface mass balance field
67 measurements from ablation stakes are sparse. Second, these measurements cannot be expected to
68 be representative given that the ice ablation exhibits a strong spatial variability depending on the
69 debris thickness or type (Azam et al., 2014; Berthier and Vincent, 2012; Hagg et al., 2008; Inoue and
70 Yoshida, 1980; Mihalcea et al., 2006), and measurements can only be made at locations where the ice
71 surface can be reached. Furthermore, geodetic measurements based on the difference between digital
72 elevation models (DEMs) derived from satellite or aerial imagery only determine surface height change



73 and glacier-wide mass balance and are typically unable to resolve the spatial pattern of surface mass
74 balance (Immerzeel et al., 2014).

75 In this paper, we assess the surface mass balance of the entire debris-covered tongue of a Himalayan
76 glacier (Changri Nup Glacier) using the ice flux method (Berthier and Vincent, 2012; Nuimura et al.,
77 2011; Nuth et al., 2012). DEMs constructed through terrestrial photogrammetry surveys in 2011 and
78 2014, an unmanned aerial vehicle (UAV) survey in 2015 and two satellite stereo pairs acquired in
79 2009 and 2014, are used to estimate changes in glacier thickness. The surface mass balance of the
80 debris-covered area is inferred from the difference between (a) the ice flux measured through a
81 cross section at the upper limit of the debris-covered area and (b) the observed elevation change.
82 Finally, we compare our robust field-based estimate of the debris-covered glacier mass balance
83 against surface mass balances observed at nearby debris-free glaciers and quantify the overall
84 reduction in ablation due to debris cover.

85

86

87 2. Site description

88 Debris-covered Changri Nup Glacier (27.987°N, 86.785°E) is located in the Dudh Koshi catchment, 14
89 km west of Mt. Everest (Figure 1). The climate in this region is monsoon dominated and 70-80% of the
90 annual precipitation falls during between June and September (Salerno et al., 2015; Wagon et al.,
91 2013). Changri Nup is a confined valley glacier with no ablation-zone tributaries. With a total length of
92 ca. 4 km and a total area of ca. 2.7 km² it presents a reasonable size for field campaigns. The
93 accumulation zone of the glacier is a cirque surrounded by high peaks reaching elevations greater than
94 6500 m asl and large serac avalanches feed the accumulation zone from steep south-facing slopes.
95 Most of the ablation zone is covered by debris, and interspersed with supraglacial ponds and ice cliffs.
96 The debris-covered portion of the tongue has a length of 2.3 km and an average width of 0.7 km, with
97 a terminus located at 5240 m asl.

98 A few hundreds of meters south-west of Changri Nup Glacier stands a smaller debris-free glacier known
99 locally as White Changri Nup Glacier (Figure 1; 27.97°N, 86.76°E). White Changri Nup Glacier has a total
100 area of 0.92 km², a north-east aspect, and it ranges in elevation from 5865 to 5335 m asl.

101 Additional mass balance data used in this study are taken from nearby Pokalde (27.9° N, 86.8° E) and
102 Mera (27.7° N, 86.9° E) glaciers, located approximately 7 and 30 km south-east of Changri Nup Glacier,
103 respectively (Wagon et al., 2013). Pokalde Glacier is a small (0.1 km²) north-facing glacier that ranges
104 in elevation from 5690 m asl to 5430 m asl. Mera Glacier is larger (5.1 km²), originates at Mera summit
105 (6420 m a.s.l.) and splits into two distinct branches at 5800 m asl. The Mera branch faces north and
106 west and extends down to 4940 m asl, whereas the Naulek branch faces north-east and terminates at
107 an elevation of 5260 m asl.

108 3. Data and Methods



109 A suite of field-based and remote sensing methods were used to calculate the mass balance of clean
110 and debris-covered Changri Nup glaciers. These included photogrammetric surveys, field-based DGPS
111 and ground penetrating radar (GPR) surveys, UAV surveys, point mass balance measurements, and
112 satellite-derived geodetic mass balances.

113 3.1. Photogrammetric surveys

114 Terrestrial photogrammetric surveys were carried out in the last week of October 2011 and in the last
115 week of November 2014. The photographs were made using a Canon EOS5D Mark II digital reflex
116 camera with Canon 50 mm f/2.8 AF fixed focus lenses. The 21.1 million pixel images are captured in
117 raw uncompressed format.

118 From three bases, oblique terrestrial photographs that covered most of the debris-covered tongue
119 were collected under similar conditions in October 2011 and November 2014. Camera positions were
120 between 1100 m and 2000 m from the glacier, which results in a ground-scaled pixel size of 0.14 to
121 0.25 m. The camera locations are 280, 264, 253 m apart and the base formed by the camera locations
122 is roughly perpendicular to the sightings. The base-to-distance ratio is about 17 % which enables a
123 good stereovision for manual plotting during restitution. These photogrammetric measurements were
124 used to build DEMs over the surface area of the glacier tongue downstream of the cross section M
125 (Figure 2). In order to geometrically correct the images, ground control points (GCP) (28 large white
126 painted crosses 2x2 m and 12 characteristic rocks) that were easily identifiable on the pictures were
127 measured using a geodetic differential global positioning system (DGPS; Figure 2). The DGPS
128 measurements have an intrinsic accuracy of +/- 0.01 m. Additional tie points (36 to 60 points depending
129 on the pair of photographs) on the overlapping images were added to improve consistency.
130 Photogrammetric restitutions were obtained using ArcGIS and ERDAS StereoAnalyst software, and the
131 actual geometric correction was performed with Leica LPS software with an estimated uncertainty of
132 0.06 m in XYZ. The accuracy of the photogrammetric restitution has been assessed from the
133 comparison between DGPS and photogrammetric measurements accrued out on 25 points not used
134 as GCPs (see section 4.3). The photogrammetric restitution was done manually and elevation contours
135 were constructed at 5 m intervals.

136

137 3.2. Ground penetrating radar measurements

138 Ground penetrating radar (GPR) measurements were performed on 25 October 2011 to measure ice
139 thickness on the transverse cross section M, located upstream of the debris-covered area at ca. 5525
140 m a.s.l. (Figure 2). We used a pulse radar system (Icefield Instruments, Canada) based on the Narod
141 transmitter (Narod and Clarke, 1994) with separate transmitter and receiver, with a frequency centred
142 near 4.2 MHz and an antenna length of 10 m. Transmitter and receiver were towed in snow sledges
143 along the transverse profile, separated by a fixed distance of 20 m, and measurements were made
144 every 10 m. The positions of the receiver and the transmitter were recorded with DGPS measurements,
145 with an accuracy of +/- 0.1 m (combination of the accuracy of the DGPS and the radar antenna
146 locations).

147 To estimate the ice depth, the speed of electromagnetic wave propagation in ice was assumed to be
148 167 m μs^{-1} (Hubbard and Glasser, 2005). Field measurements were performed in such a way as to



149 obtain reflections from the glacier bed located more or less in the vertical plane with the measurement
150 points at the glacier surface, allowing the glacier bed to be determined in two dimensions. The bedrock
151 surface was constructed as an envelope of all ellipse functions, which give all the possible reflection
152 positions between sending and receiving antennas. Estimates of bedrock depths were then migrated
153 and interpolated to reconstruct the glacier/bedrock interface in two dimensions to account for the bed
154 slope. See (Azam et al., 2012) for details of the methodology and an example of a radargram acquired
155 on Chhota Shigri Glacier (India) using the same device.

156

157 3.3. Ice flow velocities and elevation changes from DGPS measurements

158 DGPS measurements were collected on 6 transverse profiles located on the tongue of the glacier in
159 the last weeks of October 2011, November 2014, and November 2015. (Figure 2). We used dual
160 frequency Topcon devices with 1 s acquisition frequency and ~10 s acquisition time at each
161 measurement point. These measurements were performed relative to a fixed reference point outside
162 the glacier on stable ground. Maximum uncertainty is ± 0.1 m for horizontal and vertical components,
163 the horizontal uncertainty being usually lower.

164 To measure ice flow velocities, seven bamboo stakes along the debris-free cross section M (Figure 2)
165 were installed up to a depth of 6 m in 2011. Six of these stakes were replaced in 2014, and all were re-
166 surveyed in 2015. Ice flow velocities were obtained from the displacements of the stakes as well as of
167 6 painted rocks located also along the cross section M and measured between 2011 and 2015 using
168 DGPS. Ice flow velocities were also obtained in the debris-covered ablation area with DGPS
169 measurements performed on more than 75 painted or recognizable rocks in 2011, 2012, 2014 and
170 2015, and allowed us to delineate the active part of the glacier from the stagnant ice. Some
171 measurements performed on painted stones were discarded when the stones slipped on ice or rolled
172 down on steep slopes.

173

174 3.4. Unmanned Aerial Vehicle survey

175 A detailed survey of the glacier surface was conducted on 22-24 November 2015 using the senseFly
176 eBee UAV. Over the course of five survey flights, a total of 582 photos were collected with the onboard
177 Canon Ixus from an average altitude of 325 m above the glacier surface (Figure 2). Prior to the survey
178 flights, we collected DGPS measurements of 34 ground control points that consisted of (a) red fabrics
179 with painted white squares and (b) white crosses used for the photogrammetry (Figure 2). Twenty-
180 four GCPs were used to process the imagery and create a DEM with Agisoft, and 10 GCPs were reserved
181 as independent checks on the accuracy of the DEM.

182 The images from the survey were processed using the Structure for Motion (SfM) algorithm that is
183 implemented in the software package Agisoft Photoscan Professional version 1.2.0 (Agisoft, 2014).
184 First, a feature recognition and matching algorithm is applied on a set of overlapping pictures resulting
185 in a set of points in 3D space derived from the matching features and camera positions. This positioning
186 of the sparse point cloud is then corrected using the dGPS measurements. Multi-view stereo
187 techniques are then used to generate a dense point cloud of the glacier surface. This dense point cloud



188 is used to construct the DEM and in a final step the DEM is used to generate a geometrically corrected
189 mosaic of all input images. A detailed description of the processing steps can be found in Kraaijenbrink
190 et al., (2016).

191

192 Based on the 10 independent GCPs, the average error in the UAV-derived DEM is +/- 0.04 m in the
193 horizontal, and +/- 0.10 in the vertical. Removal of an outlier GCP with a vertical error of 0.7 m (the
194 GCP is located on the edge of a large boulder) reduces the average vertical error to +/- 0.08 m. The
195 resulting orthomosaic and DEM derived from UAV imagery are shown in Figure 3. Photogrammetric
196 and UAV DEMs are resampled to 5 m resolution using a krigging interpolation method before
197 estimating elevation changes.

198

199 3.5. Geodetic mass balance from satellite images

200 To calculate geodetic mass balances from satellite imagery, we used DEMs derived from two satellite
201 stereo acquisitions. The 2014 DEM was derived from two SPOT7 images acquired on 28 October 2014.
202 The ground resolution of each image is 1.5 m and the base to height ratio between the two images is
203 0.24. The images are slightly covered by snow above approximately 4800 m a.s.l. The DEM was derived
204 without ground control points (GCPs) using the commercial software PCI Geomatica 2015. The 2009
205 DEM was derived from two SPOT5 images acquired on 28 October and 4 November 2009. The ground
206 resolution of each image is 2.5 m and the base to height ratio is 0.45. The 2009 DEM was derived using
207 23 GCPs extracted from the 2014 SPOT7 DEM and the corresponding 1.5 m ortho-image. Output
208 resolution of both DEMs was set to 6 m.

209 The two DEMs were horizontally shifted to minimize the standard deviation of elevation differences
210 on stable terrain (Berthier et al., 2007). Glaciers were masked out using the inventory from (Gardelle
211 et al., 2013). We excluded the off-glacier pixels for which the elevation difference was larger the three
212 time the normalized median absolute deviation. The vertical shift between the two DEMs was
213 calculated as the median elevation difference on flat and stable zones near the glaciers (1.67 km²). The
214 horizontal shifts were -3.0 m and 2.3 m in the easting and northing, respectively. The vertical shift was
215 10.0 m.

216 The uncertainty of the elevation difference between the two DEMs is assessed from the statistical
217 distribution of the elevation differences over stable terrain (Magnússon et al., 2016; Rolstad et al.,
218 2009). The standard deviation of elevation differences on stable ground (σ_{STABLE}) is 3.6 m. The
219 decorrelation length estimated from the semi-variogram is approximately 50 m, which gives 604
220 independent pixels for the entire debris-covered tongue (n_{GLA}), 330 independent pixels for the debris-
221 covered tongue common with the photogrammetric survey ($n_{\text{GLA_COM}}$), and 668 independent pixels on
222 the stable zone (n_{STABLE}). Conservatively, we also assumed that the error was five times higher in the
223 voids of the DEM (Berthier et al., 2014), which represent $n_{\text{VOIDS}}/n_{\text{GLA}} = 6.6\%$ of the pixels for the entire
224 tongue and less than 4 % of the pixels for the area in common with the photogrammetric survey.
225 Therefore, we assumed that the total uncertainty for the glacier elevation difference could be obtained
226 as the sum of three independent error sources: the uncertainty on the median elevation difference on



227 stable zones, the standard error on the mean elevation change on glacier and an estimate of the error
228 due to voids in the DEM. By summing these three terms quadratically, we obtain:

$$229 \quad \sigma_{\text{ELEV}} = \sqrt{(\sigma_{\text{STABLE}}/n_{\text{STABLE}})^2 + (\sigma_{\text{STABLE}}/n_{\text{GLA}})^2 + \left(5 \frac{\sigma_{\text{STABLE}}}{n_{\text{GLA}}} \times \frac{n_{\text{VOIDS}}}{n_{\text{GLA}}}\right)^2} \quad [\text{Eq. 1}]$$

230 We found $\sigma_{\text{ELEV}} = 0.21$ m for the total debris-covered tongue and 0.25 m for the area overlapping with
231 the photogrammetric survey.

232

233 3.6 Point surface mass balance (SMB) measurements

234 Point SMBs, with uncertainties of +/- 0.20 m w.e., were calculated from annual stake emergences
235 recorded between 2011 and 2015 over both Changri Nup glaciers as well as Pokalde and Mera glaciers
236 (see (Wagon et al., 2013) for details of the methodology). Over Changri Nup Glacier, 7 stakes were
237 inserted along the debris-free profile M on 25 October 2011, at approximately 5525 m asl. On 29
238 November 2014, a 'stake farm' was installed over a 2400 m² area in the debris-covered tongue at an
239 elevation of 5470 m asl (Figure 2). At the 'stake farm', 13 bamboo stakes were inserted to a depth of
240 4 meters, with variable artificial debris thicknesses from 0 (bare ice) to 0.41 m. The debris composition
241 ranged from sand to decimeter-sized gravels. At White Changri Nup Glacier, 8 ablation stakes were
242 inserted to a depth of 10 m on 28-29 October 2010, at elevations ranging from 5390 m asl to 5600 m
243 asl. All these stakes on both glaciers have been measured annually, so annual surface mass balance
244 measurements are available since October 2011 except for the stake farm where only one year
245 (November 2014 - November 2015) is available.

246

247 3.7 Calculation of SMB in the debris-covered area

248 We estimate the ice flux Φ (m³ a⁻¹) through the cross section M using the cross-sectional area obtained
249 from both GPR measurements and surface DGPS survey, and the ice velocities measured at ablation
250 stakes and painted rocks along the profile. Average elevation changes (Δh) of the tongue over the
251 periods 2011-2014 and 2011-2015 are obtained from differencing the photogrammetric and UAV
252 DEMs. For the portion of Changri Nup Glacier downstream of the flux gate M, the equation of mass
253 conservation (Berthier and Vincent, 2012; Cuffey and Paterson, 2010; Reynaud et al., 1986) states that
254 the change in surface elevation (h) with time (t) between year 1 ($yr1$) and year 2 ($yr2$) is the sum of the
255 area-average surface mass balance (B) and the flux term (all terms in m ice a⁻¹):

$$256 \quad \left\langle \frac{\delta h}{\delta t} \right\rangle_{yr1-yr2} = \frac{\langle B \rangle_{yr1-yr2}}{\rho} + \frac{\Phi_{FG} - \Phi_{front}}{A} \quad [\text{Eq. 2}]$$

257 where ρ is the density of ice (900 kg m⁻³), Φ_{FG} (m³ ice a⁻¹) is the ice flux through cross section M,
258 Φ_{front} is the flux at the glacier front (equal to zero) and A (m²) is the glacier area downstream of the
259 cross section M. $\langle \frac{\Phi_{FG}}{A} \rangle_{yr1-yr2}$ is the average emergence velocity below cross section M between year
260 1 and year 2. Note that the emergence velocity refers to the upward or downward flow of ice relative
261 to the glacier surface (Cuffey and Paterson, 2010). Averaged over the entire ablation zone, it would
262 correspond to the average surface mass balance of this zone for a steady state glacier. Taking into



263 account the elevation changes of the tongue, we can calculate the area average surface mass balance
264 between 2011 and 2014, and 2011 and 2015 in this region.

265

266 4. Results

267 4.1. Ice flow velocities measurements and delineation of the tongue.

268 The demarcation between active glacier flow and stagnant glacier ice downstream of cross section M
269 is crucial for our SMB assessment (Eq. 2). However, the strongly heterogeneous debris layer covering
270 this tongue may mask the true glacier margin. Moreover, the presence of the ice beneath the debris
271 layer does not prove that this ice is connected to the active glacier. Indeed, this glacier has been in
272 retreat over the last decades and many stagnant ice areas are no longer connected to the active glacier.
273 From remote sensing optical images, it is very challenging to delineate the margins of debris-covered
274 glaciers (Paul et al., 2013). For instance, several previous studies (Quincey et al., 2009; Rowan et al.,
275 2015) have indicated that Changri Nup Glacier was connected to the Khumbu Glacier, a distance of
276 nearly 3.5 km from the terminus delineated in this study. Similarly, the inventories most commonly
277 used in this region connect the debris-covered Changri Nup, the debris-free Changri Nup and the
278 Changri Shar glaciers (Bolch et al., 2011; Gardelle et al., 2013; Nuimura et al., 2012, 2015).

279 For Changri Nup Glacier, zones of active glacier flow were delineated using horizontal velocities derived
280 from repeat dGPS measurements. Velocities derived from freely available optical imagery (e.g.
281 Landsat) cannot resolve velocities less than $5 - 10 \text{ m a}^{-1}$ (Paul et al., 2015; Quincey et al., 2009; Rowan
282 et al., 2015). The horizontal ice flow velocities range from 12.7 m a^{-1} in the vicinity of cross-section M
283 to zero close to the terminus and margins (Figure 3).

284 Despite the presence of stagnant ice far downstream of the terminus, the delineation of the terminus
285 is clear (dashed line in Figure 3). Indeed, just downstream the snout, a river is flowing on a thick layer
286 of sand in a large flat area. However, at some locations for which the glacier margin was unclear, we
287 spatially interpolated the measured ice flow velocities using a kriging interpolation method and
288 delineated the active part of the glacier at the boundary of actively flowing ice (Figure 3). With this
289 approach and obvious features in the field (slope change, visible ice), the debris-covered ablation area
290 was estimated to be 1.494 km^2 with an uncertainty of 0.16 km^2 , taking into account an uncertainty of
291 $\pm 20 \text{ m}$ on the delineation of the glacier outlines.

292 4.2. Ice flux at the upper cross section of the debris covered area and tongue- 293 averaged emergence velocity

294 The ice flux at cross section M (Fig. 2) was obtained by multiplying the surface area of this cross section
295 with the mean cross sectional ice flow velocity. From the GPR measurements (Fig. 4a), the maximum
296 observed ice thickness is 150 m, and the cross sectional area has been assessed at 79300 m^2 in 2011.
297 Taking into account the thickness decrease of 0.8 m a^{-1} at cross section M (Table 1) between 2011 and
298 2015, we calculated a mean cross sectional area of $78\,200 \text{ m}^2$.



299 A mean cross-sectional velocity can be calculated from surface velocities and assumptions about the
300 relation between mean surface velocity and depth-averaged velocity. Here, two approaches are used
301 to estimate the mean surface velocity. The first uses all surface velocities observed along the flux gate
302 between 2011 and 2015, and the mean surface velocity is calculated by fitting a second-order
303 polynomial function (Fig. 4b). Unfortunately, the surface velocities were not measured along the
304 glacier margins. We thus assume that ice flow velocity decreases linearly to zero at the margin of the
305 glacier (Fig. 4b), and obtain a mean surface velocity of 9.7 m a^{-1} from an integral calculation. The second
306 approach infers a mean surface velocity from the center-line surface velocity. The ratio between the
307 mean surface velocity and the center-line surface velocity has been estimated to be between 0.7 and
308 0.8 for other mountain glaciers (Azam et al., 2012; Berthier and Vincent, 2012). Following this
309 approach, and given that the center-line surface velocity is 12.7 m a^{-1} , the mean surface velocity is
310 assessed to $9.5 \pm 0.6 \text{ m a}^{-1}$ which is in agreement with the first estimate.

311 The next step is the conversion from mean surface velocity to depth-averaged velocity. Without basal
312 sliding, theoretical calculations suggest that the depth-averaged velocity is 80% of the mean surface
313 velocity (for $n=3$ in Glen's law; (Cuffey and Paterson, 2010), p.310). We do not have any information
314 about the thermal regime of the glacier but we assume that basal sliding is negligible. Our assumption
315 is based on the fact that the glacier is probably cold, as ice in the high-elevation accumulation area ($>$
316 6200 m asl) is transported to lower elevations primarily through serac collapses. Taking the mean
317 surface velocity from the polynomial function (9.7 m a^{-1}), we therefore assume that the depth-
318 averaged velocity is 7.8 m a^{-1} . These assumptions and their influence on the resulting uncertainties are
319 discussed in section 4.4. Mean cross-sectional velocity and cross-sectional area are multiplied to
320 compute an average annual ice flux of $609\,960 \text{ m}^3 \text{ a}^{-1}$ at cross section M over the period 2011-2015.
321 This ice flux, distributed over the mean downstream glacier area of 1.494 km^2 , corresponds to an
322 emergence ice velocity of $0.37 \text{ m w.e. a}^{-1}$.

323

324

325 4.3. Elevation changes between 2011, 2014, and 2015

326 Elevation changes are directly measured along DGPS profiles and calculated by differencing the
327 terrestrial photogrammetric and UAV-derived DEMs.

328 4.3.1. Elevation changes over the area between profiles M and N

329 For the mostly debris-free region between profiles M and N, where photogrammetric measurements
330 are not available, we calculated the elevation changes from repeat DGPS measurements along profile
331 M and N. In general, cross-glacier elevation changes in clean-ice areas are expected to be homogenous
332 (Berthier and Vincent, 2012; Fischer et al., 2005; Vincent et al., 2009). At profile M, this is confirmed
333 by the spatial homogeneity in elevation profiles between years, and the mean rate of elevation change
334 is -0.8 m a^{-1} between 2011 and 2015 at this location (Fig. 5). Along the partly debris-covered profile N,
335 elevation change between 2011 and 2015 is not as homogeneous as profile M, and the mean the rate
336 of elevation change is lower (-0.5 m a^{-1} between 2011 and 2015; Table 1). Consequently, we can
337 assume that the elevation change of this region between 2011 and 2015 is equal to the mean elevation



338 change obtained at profiles M and N, i.e. 0.65 m a^{-1} . The volume change between profiles M and N is
339 87343 m^3 over the period 2011-2015.

340 4.3.2. Elevation changes over the debris-covered area

341 Downstream of profile N, we calculated the elevation changes for two periods (2011–2014 and 2011-
342 2015) by differencing DEMs obtained from terrestrial photogrammetric measurements and UAV. Due
343 to terrain obstruction, thickness changes can be calculated for 60 % of the ablation area downstream
344 of profile N. Our results show a highly heterogeneous down-wasting pattern of the tongue of Changri
345 Nup Glacier (Fig. 5 and 6). Overall, a negative change in surface elevation is observed over the
346 monitored area. Mean elevation changes of -0.95 m a^{-1} was obtained between 2011 and 2014, and -
347 0.96 m a^{-1} between 2011 and 2015, downstream of profile N. These elevation changes are very similar
348 and correspond to a volume change of $771\,346 \text{ m}^3 \text{ a}^{-1}$ over the measured surface area over the 2011-
349 2015 period.

350 4.3.3. Area-weighted elevation and mass changes below the flux gate

351 Assuming that the thickness changes described above are representative of the total area below the
352 flux gate (below profile M), we calculate an area-weighted elevation change equal to -0.93 m a^{-1}
353 between 2011 and 2015. Assuming an ice density of 900 kg m^{-3} this corresponds to an average mass
354 loss of $-0.84 \text{ m w.e. a}^{-1}$.

355 4.3.4. Surface height change validation

356 Elevation changes obtained from photogrammetry have been validated using the DGPS
357 measurements. First, we directly compare elevations from the photogrammetric transverse profiles
358 and DGPS profiles (Fig.5), and find that the differences are generally less than 1 m. Comparisons
359 between DGPS elevations at independent GCPs (i.e. not used in the generation of photogrammetric or
360 UAV DEMs) provide further support for the elevation data used in this study. The differences between
361 DGPS and photogrammetric elevations for 25 independent GCPs near the terminus and profile R have
362 a root mean squared error (RMSE) of 0.63 m. A similar comparison between DGPS spot heights and
363 UAV-derived elevations at 10 independent points gives an RMSE of 0.25 m. Second, we compare the
364 thickness changes obtained from photogrammetric and DGPS measurements. As photogrammetric
365 measurements are incomplete along the transverse profiles due to terrain obstruction, elevation
366 changes have been compared on reduced profiles. The rate of elevation changes and the comparison
367 between photogrammetric and DGPS measurements are summarized in Table 1. This comparison
368 shows a good consistency between DGPS and photogrammetric results.

369 From these data, we conclude that (i) the photogrammetric results are consistent with DGPS
370 measurements, but (ii) repeated DGPS measurements obtained from transverse profiles are not
371 sufficient to obtain a representative mean elevation change of the tongue despite the numerous
372 profiles. This is a direct result of the high spatial variability of elevation changes in the debris-covered
373 area of the glacier.

374 In an alternative test, elevation changes outside the delineated terminus were calculated. In this region
375 with a surface area of 0.014 km^2 (not shown), average thickness changes of -0.07 m and -0.18 m were
376 observed over the periods 2011-2014 and 2011-2015, respectively. These are not significantly different



377 from zero, when the margin of error is considered. However, the unconfirmed presence of stagnant
 378 ice in the check area may lead to the slightly negative surface height changes (e.g. Figure 6c).

379 Finally, photogrammetric and UAV-derived elevation changes can be compared to elevation changes
 380 measured from the satellite stereo acquisitions between 2009 and 2014, though the period of
 381 measurement is slightly different. The mean elevation change measured from the difference between
 382 the 2014 DEM and the 2009 DEM is -0.88 m a^{-1} on the debris-covered tongues downstream of profile
 383 M (Fig. 6c). As a more reliable comparison we also calculated the mean elevation change only for areas
 384 covered by the photogrammetric and UAV surveys, and found a median elevation difference of -0.95
 385 m a^{-1} (Fig. 6c). These results are in very good agreement, although the period of measurements are
 386 slightly different. Moreover, given the uncertainty in the ground-based measurements, the satellite
 387 images results support the assumption that the elevation changes measured on 60% of the tongue are
 388 representative of the whole area.

389

390 4.4 Averaged SMB of the debris covered area and uncertainties

391 From the difference between the emergence velocity and the mean elevation changes below profile
 392 M, we deduce an average surface mass balance of $-1.21 \text{ m w.e. a}^{-1}$ between 2011 and 2015
 393 Approximately 91% of this area is debris-covered.

394 The total uncertainty in our estimated SMB is related to the delineation of the surface area of the
 395 tongue, to the elevation changes of the tongue, to the thickness of the cross section M and to the
 396 mean cross sectional velocity at cross section M. The uncertainty of this value was assessed following
 397 the calculation of the area-averaged surface mass balance (B_M).

$$398 B_M = \frac{\rho}{A} (\Delta h_1 A_1 + \Delta h_2 A_2 - S_M U) \quad [\text{Eq. 3}]$$

399 where b is the mean SMB (m w.e. a^{-1}) downstream of cross section M, ρ is the density of ice, A is the
 400 glacier area (m^2) downstream of cross section M, Δh_1 is the elevation change (m a^{-1}) between the cross
 401 sections M and N, A_1 is the surface area (m^2) between cross sections M and N, Δh_2 is the elevation
 402 change (m a^{-1}) downstream of cross section N, A_2 is the surface area (m^2) downstream the cross section
 403 N, S_M is the cross sectional area (m^2) at M, and U is the mean cross section velocity (m a^{-1}) through the
 404 flux gate M.

405 Using Equation 3, the overall squared error (σ_b^2) on the calculated SMB is given by:

406

$$407 \sigma_b^2 = \left(\frac{\rho}{A}\right)^2 (A_1^2 \sigma_{\Delta h_1}^2 + \Delta h_1^2 \sigma_{A_1}^2 + A_2^2 \sigma_{\Delta h_2}^2 + \Delta h_2^2 \sigma_{A_2}^2$$

408

$$409 + U^2 \sigma_{S_M}^2 + S_M^2 \sigma_U^2$$

$$410 + \left(\frac{1}{A}\right)^2 (\Delta h_1 A_1 + \Delta h_2 A_2 - S_M U) \sigma_A^2) \quad [\text{Eq. 4}]$$

411



412 Uncertainties relative to the delineation of the surface areas (σ_{A_1} , σ_{A_2} , and σ_A for the surface areas A_1 ,
413 A_2 , and A respectively) are assigned a value of ± 20 m on the delineation. The uncertainty $\sigma_{\Delta h_1}$ relative
414 to the elevation changes (Δh_1) is estimated to be ± 0.20 m a^{-1} , based on previous DGPS results. Satellite
415 measurements performed between 2009 and 2014 show that the mean elevation change obtained on
416 60% of the surface differs by 0.07 m from the mean elevation change calculated on the whole surface
417 area. Consequently, for our error calculations, we assumed an uncertainty $\sigma_{\Delta h_2}$ of 0.1 m relative to the
418 average elevation change Δh_2 .

419 The uncertainty relative to the cross sectional area of profile M has been assessed using an ice
420 thickness uncertainty of 10 m. Uncertainty relative to the mean cross sectional velocity is assumed to
421 be 10% of the calculated velocity (Huss et al., 2007). Finally, the overall error σ_o on the calculated SMB
422 is 0.2 m w.e. a^{-1} .

423 5. Discussion

424 5.1. Spatial variability of elevation changes over the debris-covered tongue of 425 Changri Nup Glacier

426 High-resolution surface elevation changes derived in this study from photogrammetry, UAV surveys,
427 and satellite stereo-pairs highlight the fact that elevation changes over debris-covered glaciers are
428 highly spatially variable (Figure 6). This is already well known over debris-covered glaciers where
429 elevation changes depend on both debris thickness spatial variability and the spatial distribution of
430 ponds or cliffs (Immerzeel et al., 2014; Nuimura et al., 2012). However, this study shows that neither
431 repeat DGPS measurements obtained from transverse profiles nor an ablation stake network are
432 sufficient to obtain a representative mean elevation change or surface mass balance over debris-
433 covered glaciers. The spatial variability in height changes (Fig. 6) also precludes comparisons between
434 direct (glaciological) observations of SMB on clean and debris-covered glaciers.

435 5.2. The debris cover controversy: SMBs over debris-covered and clean-ice glaciers in 436 the Khumbu area

437 The overall surface lowering rates and mass balances of debris covered glaciers remains controversial.
438 Several recent studies showed that elevation changes on debris-covered and debris-free glaciers are
439 similar in the Himalaya and Karakoram (Gardelle et al., 2013; Kääb et al., 2012; Pellicciotti et al., 2015).
440 Conversely, (Nuimura et al., 2012) showed that the debris-covered areas are subject to higher rates of
441 lowering than debris-free areas in Khumbu region, though the 400 m difference in mean elevation
442 between the debris-covered and debris free areas (5102 and 5521 m asl, respectively) may account for
443 this conclusion.

444 Comparisons between the mass balances of debris-covered and debris-free glaciers (as opposed to
445 comparisons of surface elevation change only) are hindered by methodological deficiencies and
446 uncertainties. First, geodetic studies typically provide only glacier- or region-wide mass balances based
447 on elevation changes (Bolch et al., 2008, 2011; Nuimura et al., 2012). As accumulation zones are not
448 debris-covered, these methods are unable to determine a separate surface mass balance for debris-
449 covered areas, because they do not account for the emergence velocity. Moreover, the size, altitude



450 and dynamic behavior of clean and debris-covered glaciers are different and the comparison between
451 glacier-wide mass balances cannot distinguish ablation rates between debris-covered and debris-free
452 areas. In addition, most of these studies in Nepal have been carried out on catchments with a
453 predominance of debris-covered glaciers (Bolch et al., 2011) and do not enable a relevant comparison
454 with entirely debris-free glaciers. Second, the uncertainties related to these remote sensing methods
455 (e.g. the delineation of the glaciers, elevation bias due to the radar penetration into the ice, elevation
456 change assessment and snow density) are large (Pellicciotti et al., 2015). Finally, the regional average
457 mass balances obtained from geodetic methods mask strong differences among glaciers and cannot
458 be used to infer conclusions on the ablation rate comparison between debris-covered and debris-free
459 ice.

460 In contrast with full-glacier geodetic results, our method based on ice flux calculations and surface
461 lowering observations from photogrammetric and UAV DEMs enables the calculation of an average
462 SMB (-1.21 ± 0.2 m w.e. a^{-1}) over the whole debris-covered tongue of Changri Nup Glacier. This
463 assessment includes an area of nearly debris-free ice between the profiles M and N. However, this area
464 represents less than 9% of the total surface area below profile M, and we can consider that the
465 obtained surface mass balance value is representative of the debris-covered area for the periods 2009-
466 2014, 2011-2014 and 2011-2015.

467 As our estimate of SMB incorporates the spatial variability in surface lowering, we compare the area-
468 averaged SMB obtained for Changri Nup Glacier with direct SMB measurements from debris-free ice
469 and glaciers in the region (Figure 7). These include point SMB measurements from profile M (Figure 2),
470 White Changri Nup Glacier (5390 to 5600 m asl), Pokalde Glacier (5505 to 5636 m asl), and Mera and
471 Naulek glaciers (5112 to 5415 m asl). Also displayed on Figure 7 are the 2014-15 point SMB
472 measurements from the stake farm located in the debris-covered area of Changri Nup Glacier (Figure
473 2).

474 The average SMB assessed over the debris-covered Changri Nup Glacier tongue (-1.21 ± 0.2 m w.e. a^{-1})
475 is similar to directly observed SMBs at profile M (-1.50 and -0.85 m w.e. a^{-1}), and less negative than
476 measurements from the stake farm (-1.35 to -1.98 m w.e. a^{-1}). This implies that (i) the average SMB of
477 the tongue would be much lower if it was debris-free, and that (ii) the stake farm measurements are
478 not representative of melt rates over the rest of the debris-covered area. The mean vertical gradient
479 of SMB from and the nearby White Changri Nup Glaciers is equal to 1.4 ± 0.5 m w.e. $(100 \text{ m})^{-1}$ (Fig. 7).
480 Applying this gradient to the mean observed SMB at profile M (1.16 m w.e. a^{-1}), we estimate that a
481 SMB of -3.0 m w.e. a^{-1} for debris-free ice at 5380 m asl, i.e. the mean altitude of the debris covered
482 area. This theoretical SMB averaged over the whole Changri Nup tongue (assuming no debris-cover)
483 has been obtained by multiplying every 50-m altitudinal area by its corresponding SMB (derived from
484 the White Changri Nup vertical SMB intercepting the mean SMB at profile M), summing them over the
485 tongue and dividing by the total tongue area. The difference between two (1.8 ± 0.6 m w.e. a^{-1})
486 represents the overall reduction in melt due to debris cover.

487

488

489



490

491 Several studies have suggested that supraglacial ponds and ice cliffs considerably enhance glacier
492 ablation for debris covered glaciers (Benn et al., 2012; Brun et al., 2016; Buri et al., 2015; Miles et al.,
493 2015; Sakai et al., 2000; Zhang et al., 2011). Although supraglacial ponds and ice cliffs are present on
494 the debris covered tongue of the Changri Nup Glacier, the overall mass loss is still considerably reduced
495 due to the debris cover and we conclude that the insulating effect dominates at this site.

496 This conclusion seems to contradict the results of (Gardelle et al., 2013; Kääb et al., 2012) which
497 revealed comparable rates of elevation changes on debris covered and clean ice glaciers. However,
498 these previous results came from geodetic measurements that cannot (or hardly) account for the
499 effect of ice dynamics (i.e. difference in emergence velocities between debris-covered and clean-ice
500 glaciers). To overcome this issue, (Kääb et al., 2012) compared elevation changes between debris-
501 covered and clean ice using neighboring ICESat footprints (separated by approximately 1 km), in an
502 attempt to minimize differences in emergence velocity. Still, the geodetic method does not permit
503 direct comparisons of ablation rate, and only the ice flux method employed here allows for reliable
504 estimate of tongue-wide mass balance and comparisons with other glaciers.

505 6. Conclusions

506 The calculated surface mass balance of the debris-covered area of Changri Nup Glacier has been
507 obtained from (i) ice flux at a cross section close to the boundary between debris-free area and debris-
508 covered area and (ii) elevation changes of the tongue. From the calculated ice flux we estimate an
509 average emergence velocity for the debris-covered tongue of $+0.37 \text{ m w.e. a}^{-1}$. The average surface
510 elevation change between 2011 and 2015, derived from photogrammetric and UAV DEMs, is equal to
511 $-0.84 \text{ m w.e. a}^{-1}$. Consequently, the average emergence velocity does not compensate the surface
512 mass balance, and we infer an average SMB of $-1.21 \pm 0.20 \text{ m w.e. a}^{-1}$ over the debris-covered area of
513 Changri Nup Glacier (5240-5525 m asl).

514 A vertical mass balance gradient derived from nearby debris-free glaciers suggests that the average
515 SMB would be $-3.0 \text{ m w.e. a}^{-1}$ if the glacier was debris-free. This net mass loss reduction of 1.8 ± 0.6
516 m w.e. a^{-1} indicates that the surface mass balance is strongly influenced by the debris cover. The
517 insulation effect of debris cover largely dominates the enhanced ice ablation due to supra-glacial ponds
518 and exposed ice cliffs at this site.

519 Our method to obtain the surface mass balance of the debris-covered area is reliable. However, the
520 application of the method requires accurate and extensive field data and is hard to transpose to
521 numerous or larger glaciers. Indeed, a precise delineation of the debris-covered glacier tongue is
522 required. For this purpose, ice flow velocities determinations with DGPS field measurements are
523 needed given that ice flow velocities are very low in the debris-covered areas in the vicinity of the
524 margins. In addition, GPR measurements performed on a transverse cross section located upstream
525 the debris covered area are also mandatory.

526 Our results have major implications for studies modeling the future evolution of debris-covered
527 glaciers (Rowan et al., 2015; Shea et al., 2015). An empirical model of debris-covered glacier melt that



528 takes into consideration the relevant processes (surface melt, englacial/subglacial melt, and ice cliff
529 migration and density) will be an important development.

530 **Acknowledgments:**

531 This work has been supported by the French Service d'Observation GLACIOCLIM, the French National
532 Research Agency (ANR) through ANR-09-CEP-005-01-PAPRIKA, and ANR-13-SENV-0005-04-PRESHINE,
533 and has been supported by a grant from Labex OSUG@2020 (Investissements d'avenir – ANR10
534 LABX56). This study was carried out within the framework of the Ev-K2-CNR Project in collaboration
535 with the Nepal Academy of Science and Technology as foreseen by the Memorandum of
536 Understanding between Nepal and Italy, and thanks to contributions from the Italian National
537 Research Council, the Italian Ministry of Education, University and Research and the Italian Ministry of
538 Foreign Affairs. Funding for the UAV survey was generously provided by the United Kingdom
539 Department for International Development (DFID) and by the Ministry of Foreign Affairs, Government
540 of Norway. This project has received funding from the European Research Council (ERC) under the
541 European Union's Horizon 2020 research and innovation programme (grant agreement No 676819).
542 EB acknowledges support from the French Space Agency (CNES) through the TOSCA Top Glaciers
543 project. SPOT5 HRG images were obtained thanks to ISIS-CNES project #510. This work was supported
544 by public funds received in the framework of GEOSUD, a project (ANR-10-EQPX-20) of the program
545 "Investissements d'Avenir" managed by the French National Research Agency. The International
546 Centre for Integrated Mountain Development is funded in part by the governments of Afghanistan,
547 Bangladesh, Bhutan, China, India, Myanmar, Nepal, and Pakistan. The views expressed are those of the
548 authors and do not necessarily reflect their organizations or funding institutions.

549

550 **References:**

551

552 Agisoft: PhotoScan Professional 1.0.0 user manual., St Petersburg., 2014.

553 Azam, M. F., Wagnon, P., Ramanathan, A., Vincent, C., Sharma, P., Arnaud, Y., Linda, A., Pottakkal, J.
554 G., Chevallier, P., Singh, V. B. and Berthier, E.: From balance to imbalance: a shift in the dynamic
555 behaviour of Chhota Shigri glacier, western Himalaya, India, *J. Glaciol.*, 58, 315–324,
556 doi:10.3189/2012JoG11J123, 2012.

557 Azam, M. F., Wagnon, P., Vincent, C., Ramanathan, A., Linda, A. and Singh, V. B.: Reconstruction of the
558 annual mass balance of Chhota Shigri glacier, Western Himalaya, India, since 1969, *Ann. Glaciol.*, 55,
559 69–80, doi:10.3189/2014AoG66A104, 2014.

560 Benn, D. I., Bolch, T., Hands, K., Gulle, J., Luckman, A., Nicholson, L. I., Quincey, D., Thompson, S.,
561 Toumi, R. and Wiseman, S.: Response of debris-covered glaciers in the Mount Everest region to recent
562 warming, and implications for outburst flood hazards, *Earth-Sci. Rev.*, 114(1-2), 156–174,
563 doi:10.1016/j.earscirev.2012.03.008, 2012.



- 564 Berthier, E. and Vincent, C.: Relative contribution of surface mass-balance and ice-flux changes to the
565 accelerated thinning of Mer de Glace, French Alps, over 1979-2008, *J. Glaciol.*, 58, 501–512,
566 doi:10.3189/2012JG11J083, 2012.
- 567 Berthier, E., Arnaud, Y., Kumar, R., Ahmad, S., Wagnon, P. and Chevallier, P.: Remote sensing estimates
568 of glacier mass balances in the Himachal Pradesh (Western Himalaya, India), *Remote Sens. Environ.*,
569 108(3), 327–338, doi:10.1016/j.rse.2006.11.017, 2007.
- 570 Berthier, E., Vincent, C., Magnússon, E., Gunnlaugsson, Á. P., Pitte, P., Le Meur, E., Masiokas, M., Ruiz,
571 L., Pálsson, F., Belart, J. M. C. and Wagnon, P.: Glacier topography and elevation changes derived from
572 Pléiades sub-meter stereo images, *The Cryosphere*, 8(6), 2275–2291, doi:10.5194/tc-8-2275-2014,
573 2014.
- 574 Bhambri, R., Bolch, T., Chaujar, R. K. and Kulshreshtha, S. C.: Glacier changes in the Garhwal Himalaya,
575 India, from 1968 to 2006 based on remote sensing, *J. Glaciol.*, 57, 543–556,
576 doi:10.3189/002214311796905604, 2011.
- 577 Bolch, T., Buchroithner, M., Pieczonka, T. and Kunert, A.: Planimetric and volumetric glacier changes in
578 the Khumbu Himal, Nepal, since 1962 using Corona, Landsat TM and ASTER data, *J. Glaciol.*, 54, 592–
579 600, doi:10.3189/002214308786570782, 2008.
- 580 Bolch, T., Pieczonka, T. and Benn, D. I.: Multi-decadal mass loss of glaciers in the Everest area (Nepal
581 Himalaya) derived from stereo imagery, *The Cryosphere*, 5(2), 349–358, doi:10.5194/tc-5-349-2011,
582 2011.
- 583 Brock, B. W., Mihalcea, C., Kirkbride, M. P., Diolaiuti, G., Cutler, M. E. J. and Smiraglia, C.: Meteorology
584 and surface energy fluxes in the 2005-2007 ablation seasons at the Miage debris-covered glacier, Mont
585 Blanc Massif, Italian Alps, *J. Geophys. Res. Atmospheres*, 115, D09106, doi:10.1029/2009JD013224,
586 2010.
- 587 Brun, F., Buri, P., Miles, E. S., Wagnon, P., Steiner, J. F., Berthier, E., Ragetti, S., Kraaijenbrink, P.,
588 Immerzeel, W. W. and Pellicciotti, F.: Quantifying volume loss from ice cliffs on debris-covered glaciers
589 using high resolution terrestrial and aerial photogrammetry, *J. Glaciol. Accept.*, 2016.
- 590 Buri, P., Pellicciotti, F., Steiner, J. F., Miles, E. S. and Immerzeel, W. W.: A grid-based model of
591 backwasting of supraglacial ice cliffs on debris-covered glaciers, *Ann. Glaciol. Accept.*, 2015.
- 592 Cuffey, K. M. and Paterson, W. S. B.: *The physics of glaciers*, Academic Press., 2010.
- 593 Fischer, U. H., Braun, A., Bauder, A. and Flowers, G. E.: Changes in geometry and subglacial drainage
594 derived from digital elevation models: Unteraargletscher, Switzerland, 1927–97, *Ann. Glaciol.*, 40, 20–
595 24, doi:10.3189/172756405781813528, 2005.
- 596 Gardelle, J., Berthier, E., Arnaud, Y. and Kääb, A.: Region-wide glacier mass balances over the Pamir-
597 Karakoram-Himalaya during 1999-2011, *The Cryosphere*, 7(4), 1263–1286, doi:10.5194/tc-7-1263-
598 2013, 2013.
- 599 Hagg, W., Mayer, C., Lambrecht, A. and Helm, A.: Sub-debris melt rates on southern Inylchek Glacier,
600 central Tian Shan, *Geogr. Ann. Ser. Phys. Geogr.*, 90(1), 55–63, doi:10.1111/j.1468-0459.2008.00333.x,
601 2008.



- 602 Hubbard, B. and Glasser, N. F.: Field techniques in glaciology and glacial geomorphology, John Wiley &
603 Sons., 2005.
- 604 Huss, M., Sugiyama, S., Bauder, A. and Funk, M.: Retreat Scenarios of Unteraargletscher, Switzerland,
605 Using a Combined Ice-Flow Mass-Balance Model, *Arct. Antarct. Alp. Res.*, 39(3), 422–431,
606 doi:10.1657/1523-0430(06-036)[HUSS]2.0.CO;2, 2007.
- 607 Immerzeel, W. W., Kraaijenbrink, P. D. A., Shea, J. M., Shrestha, A. B., Pellicciotti, F., Bierkens, M. F. P.
608 and de Jong, S. M.: High-resolution monitoring of Himalayan glacier dynamics using unmanned aerial
609 vehicles, *Remote Sens. Environ.*, 150, 93–103, doi:10.1016/j.rse.2014.04.025, 2014.
- 610 Inoue, J. and Yoshida, M.: Ablation and heat exchange over the Khumbu Glacier, *J. Jpn. Assoc. Snow*
611 *Ice*, 41(Special), 26–33, 1980.
- 612 Jouvét, G., Huss, M., Funk, M. and Blatter, H.: Modelling the retreat of Grosser Aletschgletscher,
613 Switzerland, in a changing climate, *J. Glaciol.*, 57, 1033–1045, doi:10.3189/002214311798843359,
614 2011.
- 615 Kääb, A., Berthier, E., Nuth, C., Gardelle, J. and Arnaud, Y.: Contrasting patterns of early twenty-first-
616 century glacier mass change in the Himalayas, *Nature*, 488(7412), 495–498, doi:10.1038/nature11324,
617 2012.
- 618 Kayastha, R. B., Takeuchi, Y., Nakawo, M. and Ageta, Y.: Practical prediction of ice melting beneath
619 various thickness of debris cover on Khumbu Glacier, Nepal, using a positive degree-day factor, *IAHS*
620 *Publ.*, 71–82, 2000.
- 621 Kirkbride, M. P. and Deline, P.: The formation of supraglacial debris covers by primary dispersal from
622 transverse englacial debris bands, *Earth Surf. Process. Landf.*, 38(15), 1779–1792,
623 doi:10.1002/esp.3416, 2013.
- 624 Kraaijenbrink, P., Meijer, S. W., Shea, J. M., Pellicciotti, F., Jong, S. M. D. and Immerzeel, W. W.:
625 Seasonal surface velocities of a Himalayan glacier derived by automated correlation of unmanned
626 aerial vehicle imagery, *Ann. Glaciol.*, 57(71), 103–113, doi:10.3189/2016aog71a072, 2016.
- 627 Lambrecht, A., Mayer, C., Hagg, W., Popovnin, V., Rezepkin, A., Lomidze, N. and Svanadze, D.: A
628 comparison of glacier melt on debris-covered glaciers in the northern and southern Caucasus, *The*
629 *Cryosphere*, 5, 525–538, doi:10.5194/tc-5-525-2011, 2011.
- 630 Lejeune, Y., Bertrand, J.-M., Wagnon, P. and Morin, S.: A physically based model of the year-round
631 surface energy and mass balance of debris-covered glaciers, *J. Glaciol.*, 59, 327–344,
632 doi:10.3189/2013JoG12J149, 2013.
- 633 Lutz, A. F., Immerzeel, W. W., Shrestha, A. B. and Bierkens, M. F. P.: Consistent increase in High Asia's
634 runoff due to increasing glacier melt and precipitation, *Nat. Clim Change*, 4(7), 587–592, 2014.
- 635 Magnússon, E., Muñoz-Cobo Belart, J., Pálsson, F., Ágústsson, H. and Crochet, P.: Geodetic mass
636 balance record with rigorous uncertainty estimates deduced from aerial photographs and lidar data -
637 Case study from Drangajökull ice cap, NW Iceland, *The Cryosphere*, 10(1), 159–177, doi:10.5194/tc-10-
638 159-2016, 2016.



- 639 Mattson, L.: Ablation on debris covered glaciers: an example from the Rakhiot Glacier, Panjab,
640 Himalaya, IAHS Publ., 218, 289–296, 1993.
- 641 Mihalcea, C., Mayer, C., Diolaiuti, G., Lambrecht, A., Smiraglia, C. and Tartari, G.: Ice ablation and
642 meteorological conditions on the debris-covered area of Baltoro glacier, Karakoram, Pakistan, Ann.
643 Glaciol., 43, 292–300, doi:10.3189/172756406781812104, 2006.
- 644 Miles, E. S., Willis, I., Pellicciotti, F., Steiner, J. F., Buri, P. and Arnold, N.: Refined energy-balance
645 modelling of a supraglacial pond, Langtang Khola, Nepal, Ann. Glaciol. Accept., 2015.
- 646 Nakawo, M. and Young, G. J.: Field experiments to determine the effect of a debris layer on ablation
647 of glacier ice, Ann. Glaciol., 2, 85–91, doi:10.3189/172756481794352432, 1981.
- 648 Narod, B. B. and Clarke, G. K. C.: Miniature high-power impulse transmitter for radio-echo sounding, J.
649 Glaciol., 40, 190–194, 1994.
- 650 Nicholson, L. and Benn, D. I.: Calculating ice melt beneath a debris layer using meteorological data, J.
651 Glaciol., 52, 463–470, doi:10.3189/172756506781828584, 2006.
- 652 Nuimura, T., Fujita, K., Fukui, K., Asahi, K., Aryal, R. and Ageta, Y.: Temporal Changes in Elevation of the
653 Debris-Covered Ablation Area of Khumbu Glacier in the Nepal Himalaya since 1978, Arct. Antarct. Alp.
654 Res., 43(2), 246–255, doi:10.1657/1938-4246-43.2.246, 2011.
- 655 Nuimura, T., Fujita, K., Yamaguchi, S. and Sharma, R. R.: Elevation changes of glaciers revealed by
656 multitemporal digital elevation models calibrated by GPS survey in the Khumbu region, Nepal
657 Himalaya, 1992-2008, J. Glaciol., 58(210), 648–656, doi:10.3189/2012JG11J061, 2012.
- 658 Nuimura, T., Sakai, A., Taniguchi, K., Nagai, H., Lamsal, D., Tsutaki, S., Kozawa, A., Hoshina, Y., Takenaka,
659 S., Omiya, S., Tsunematsu, K., Tshering, P. and Fujita, K.: The GAMDAM glacier inventory: a quality-
660 controlled inventory of Asian glaciers, The Cryosphere, 9(3), 849–864, doi:10.5194/tc-9-849-2015,
661 2015.
- 662 Nuth, C., Schuler, T. V., Kohler, J., Altena, B. and Hagen, J. O.: Estimating the long-term calving flux of
663 Kronebreen, Svalbard, from geodetic elevation changes and mass-balance modelling, J. Glaciol., 58,
664 119–133, doi:10.3189/2012JG11J036, 2012.
- 665 Østrem, G.: Ice Melting under a Thin Layer of Moraine, and the Existence of Ice Cores in Moraine
666 Ridges, Geogr. Ann., 41(4), pp. 228–230, 1959.
- 667 Paul, F., Barrand, N. E., Baumann, S., Berthier, E., Bolch, T., Casey, K., Frey, H., Joshi, S. P., Konovalov,
668 V., Le Bris, R., Mölg, N., Nosenko, G., Nuth, C., Pope, A., Racoviteanu, A., Rastner, P., Raup, B., Scharer,
669 K., Steffen, S. and Winsvold, S.: On the accuracy of glacier outlines derived from remote-sensing data,
670 Ann. Glaciol., 54, 171–182, doi:10.3189/2013AoG63A296, 2013.
- 671 Paul, F., Bolch, T., Kääb, A., Nagler, T., Nuth, C., Scharer, K., Shepherd, A., Strozzi, T., Ticconi, F.,
672 Bhambri, R., Berthier, E., Bevan, S., Gourmelen, N., Heid, T., Jeong, S., Kunz, M., Lauknes, T. R.,
673 Luckman, A., Boncori, J. P. M., Moholdt, G., Muir, A., Neelmeijer, J., Rankl, M., VanLooy, J. and Niel, T.
674 V.: The glaciers climate change initiative: Methods for creating glacier area, elevation change and
675 velocity products, Remote Sens. Environ., 162, 408 – 426,
676 doi:http://dx.doi.org/10.1016/j.rse.2013.07.043, 2015.



- 677 Pellicciotti, F., Stephan, C., Miles, E., Herreid, S., Immerzeel, W. W. and Bolch, T.: Mass-balance changes
678 of the debris-covered glaciers in the Langtang Himal, Nepal, from 1974 to 1999, *J. Glaciol.*, 61(226),
679 373–386, doi:10.3189/2015jog13j237, 2015.
- 680 Quincey, D. J., Luckman, A. and Benn, D.: Quantification of Everest region glacier velocities between
681 1992 and 2002, using satellite radar interferometry and feature tracking, *J. Glaciol.*, 55, 596–606,
682 doi:10.3189/002214309789470987, 2009.
- 683 Ragetti, S., Pellicciotti, F., Immerzeel, W. W., Miles, E. S., Petersen, L., Heynen, M., Shea, J. M., Stumm,
684 D., Joshi, S. and Shrestha, A.: Unraveling the hydrology of a Himalayan catchment through integration
685 of high resolution in situ data and remote sensing with an advanced simulation model, *Adv. Water*
686 *Resour.*, 78(0), 94–111, doi:10.1016/j.advwatres.2015.01.013, 2015.
- 687 Reid, T. D. and Brock, B. W.: An energy-balance model for debris-covered glaciers including heat
688 conduction through the debris layer, *J. Glaciol.*, 56, 903–916, doi:10.3189/002214310794457218,
689 2010.
- 690 Reynaud, L., Vallon, M. and Letréguilly, A.: Mass-balance measurements: problems and two new
691 methods of determining variations, *J. Glaciol.*, 32, 446–454, 1986.
- 692 Rolstad, C., Haug, T. and Denby, B.: Spatially integrated geodetic glacier mass balance and its
693 uncertainty based on geostatistical analysis: application to the western Svartisen ice cap, Norway, *J.*
694 *Glaciol.*, 55(192), 666–680, doi:10.3189/002214309789470950, 2009.
- 695 Rowan, A. V., Egholm, D. L., Quincey, D. J. and Glasser, N. F.: Modelling the feedbacks between mass
696 balance, ice flow and debris transport to predict the response to climate change of debris-covered
697 glaciers in the Himalaya, *Earth Planet. Sci. Lett.*, 430, 427–438, doi:10.1016/j.epsl.2015.09.004, 2015.
- 698 Sakai, A., Takeuchi, N., Fujita, K. and Nakawo, M.: Role of supraglacial ponds in the ablation process of
699 a debris-covered glacier in the Nepal Himalayas, *Debris-Cover. Glaciers Proc. Workshop Held Seattle*
700 *Wash. USA Sept. 2000*, 265, 2000.
- 701 Salerno, F., Guyennon, N., Thakuri, S., Viviano, G., Romano, E., Vuillermoz, E., Cristofanelli, P., Stocchi,
702 P., Agrillo, G., Ma, Y. and Tartari, G.: Weak precipitation, warm winters and springs impact glaciers of
703 south slopes of Mt. Everest (central Himalaya) in the last 2 decades (1994-2013), *The Cryosphere*, 9,
704 1229–1247, doi:10.5194/tc-9-1229-2015, 2015.
- 705 Schmidt, S. and Nüsser, M.: Fluctuations of Raikot Glacier during the past 70 years: a case study from
706 the Nanga Parbat massif, northern Pakistan, *J. Glaciol.*, 55, 949–959,
707 doi:10.3189/002214309790794878, 2009.
- 708 Shea, J. M., Immerzeel, W. W., Wagnon, P., Vincent, C. and Bajracharya, S.: Modelling glacier change
709 in the Everest region, Nepal Himalaya, *The Cryosphere*, 9(3), 1105–1128, doi:10.5194/tc-9-1105-2015,
710 2015.
- 711 Shukla, A., Gupta, R. P. and Arora, M. K.: Estimation of debris cover and its temporal variation using
712 optical satellite sensor data: a case study in Chenab basin, Himalaya, *J. Glaciol.*, 55, 444–452,
713 doi:10.3189/002214309788816632, 2009.



- 714 Thakuri, S., Salerno, F., Smiraglia, C., Bolch, T., D'Agata, C., Viviano, G. and Tartari, G.: Tracing glacier
715 changes since the 1960s on the south slope of Mt. Everest (central Southern Himalaya) using optical
716 satellite imagery, *The Cryosphere*, 8(4), 1297–1315, doi:10.5194/tc-8-1297-2014, 2014.
- 717 Vincent, C., Soruco, A., Six, D. and Le Meur, E.: Glacier thickening and decay analysis from 50 years of
718 glaciological observations performed on Glacier d'Argentière, Mont Blanc area, France, *Ann. Glaciol.*,
719 50, 73–79, doi:10.3189/172756409787769500, 2009.
- 720 Wagon, P., Vincent, C., Arnaud, Y., Berthier, E., Vuillermoz, E., Gruber, S., Ménégoz, M., Gilbert, A.,
721 Dumont, M., Shea, J. M., Stumm, D. and Pokhrel, B. K.: Seasonal and annual mass balances of Mera
722 and Pokalde glaciers (Nepal Himalaya) since 2007, *The Cryosphere*, 7(6), 1769–1786, doi:10.5194/tc-
723 7-1769-2013, 2013.
- 724 Zhang, Y., Fujita, K., Liu, S., Liu, Q. and Nuimura, T.: Distribution of debris thickness and its effect on ice
725 melt at Hailuoguo glacier, southeastern Tibetan Plateau, using in situ surveys and ASTER imagery, *J.*
726 *Glaciol.*, 57, 1147–1157, doi:10.3189/002214311798843331, 2011.



727

728 *Table 1: Mean elevation changes ($m a^{-1}$) estimated from repeat DGPS measurements and DEM*
 729 *differencing (photogrammetry, UAV and satellite) on cross sections, and over the debris-covered*
 730 *tongue (entire and common areas).*

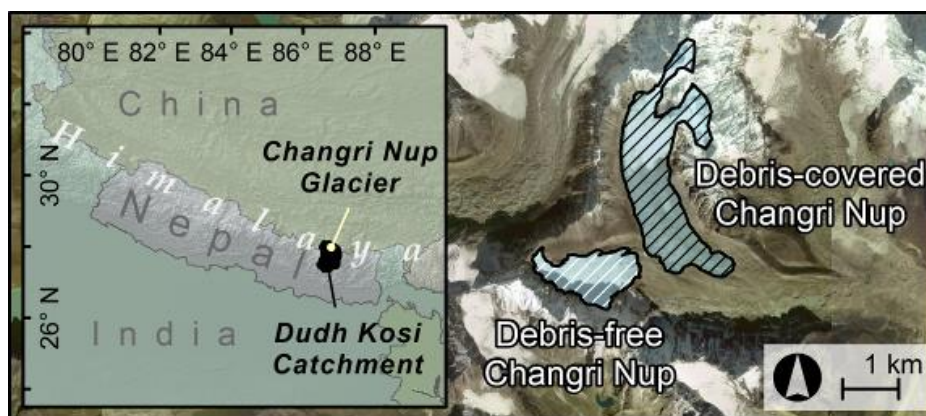
Elevation change ($m a^{-1}$)	M	N	R	P	V	Z	Tongue (whole)	Tongue (common)
DGPS 2011-2014	-0.7		-0.2	-1.3		-0.3		
Photogrammetry 2011-2014			-0.1	-1.4	-1.2	-0.2		
DGPS 2011-2015	-0.8	-0.5						
Photogrammetry and UAV survey 2011-2015			-0.2	-1.1	-1.1	-0.2		-0.96
Stereo-pair Satellite 2009-2014							-0.88	-0.95

731



732

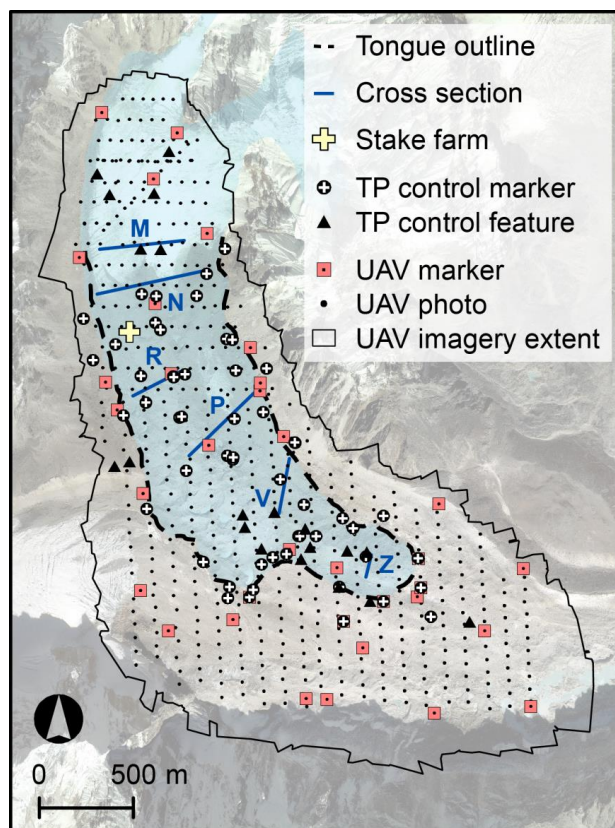
733



734

735 *Figure 1: Study area overview showing the general location (inset map) and delineation debris-free*
736 *and debris-covered Changri Nup glaciers. Background is from ESRI basemap imagery.*

737

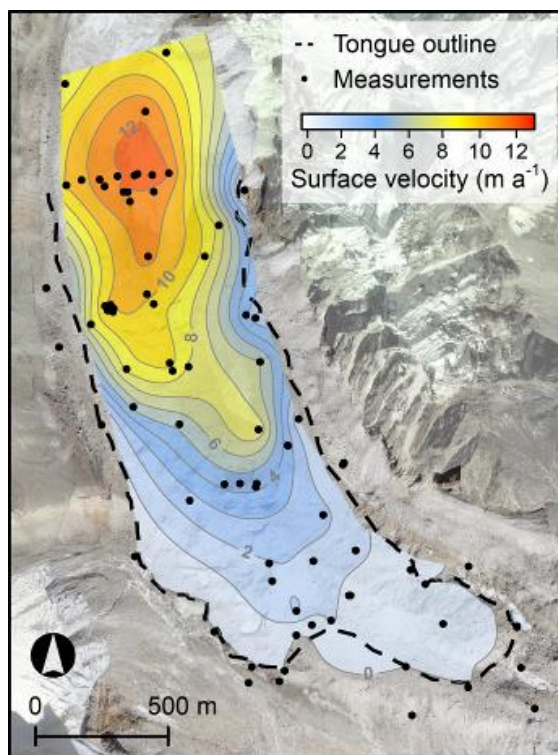


738

739 *Figure 2: Map of debris-covered Changri Nup Glacier showing the glacierized area (light blue), DGPS*
740 *cross sections (blue), delineated debris-covered tongue (dashed black line), and UAV imagery extent*
741 *(black line). TP = terrestrial photogrammetry, and background is from ESRI basemap imagery. TP*
742 *control markers are painted crosses, and TP control features are characteristic boulders.*

743

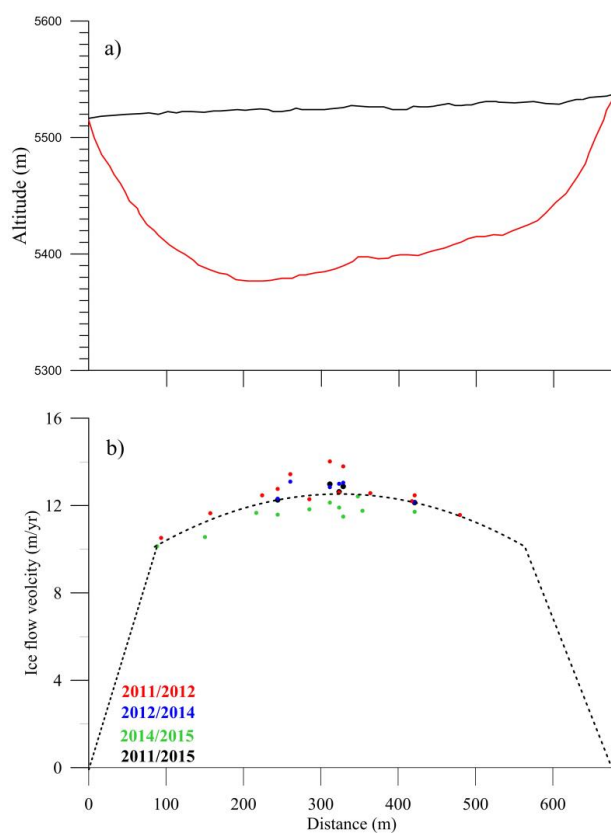
744



745

746 *Figure 3: Map of measured glacier surface velocities (m a^{-1}), and location of the glacier margins*
747 *(dashed line).*

748



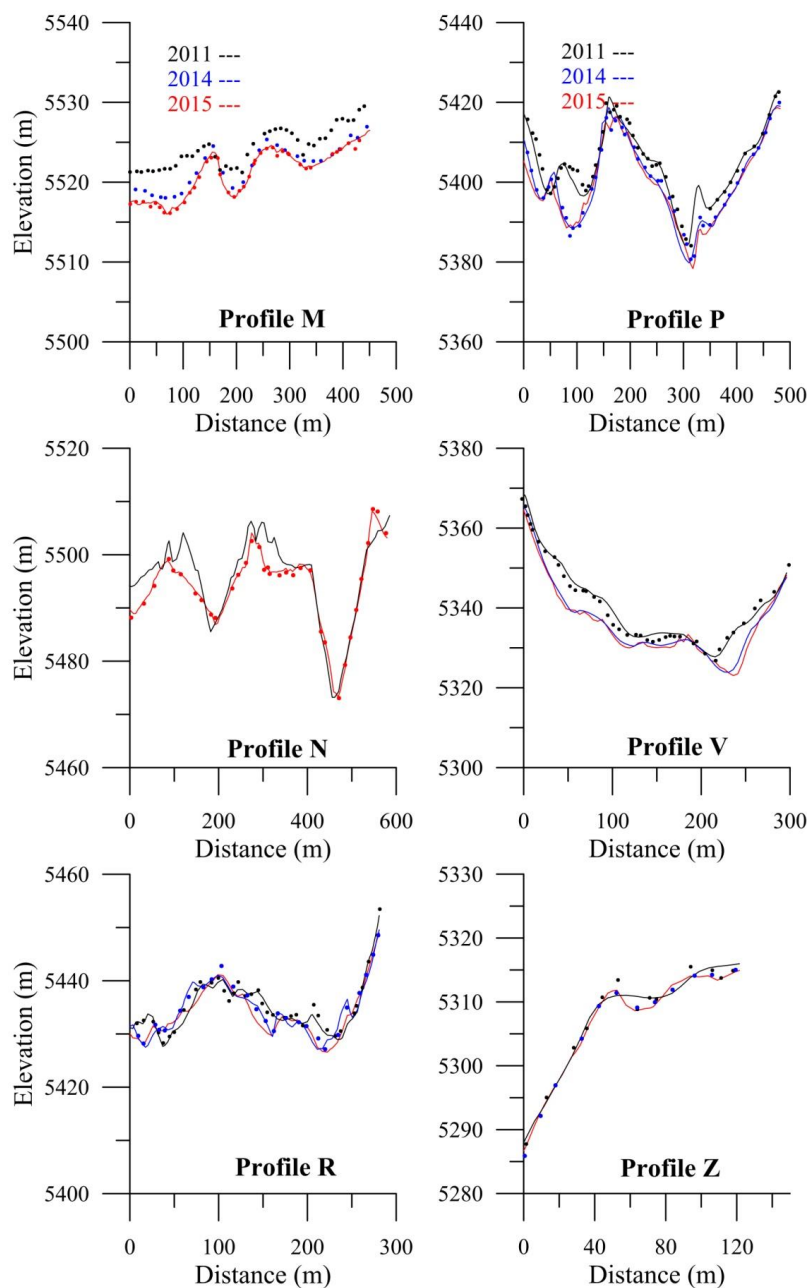
749

750

751 *Figure 4: a) Cross section of glacier thickness derived from GPR measurements at profile M on 25*
752 *October 2011, b) Measured surface velocities across section M over the period 2011-2015. The dashed*
753 *line corresponds to a polynomial function with a degree 2 using all the measurements and forced*
754 *linearly to zero at the right and left margins.*

755

756



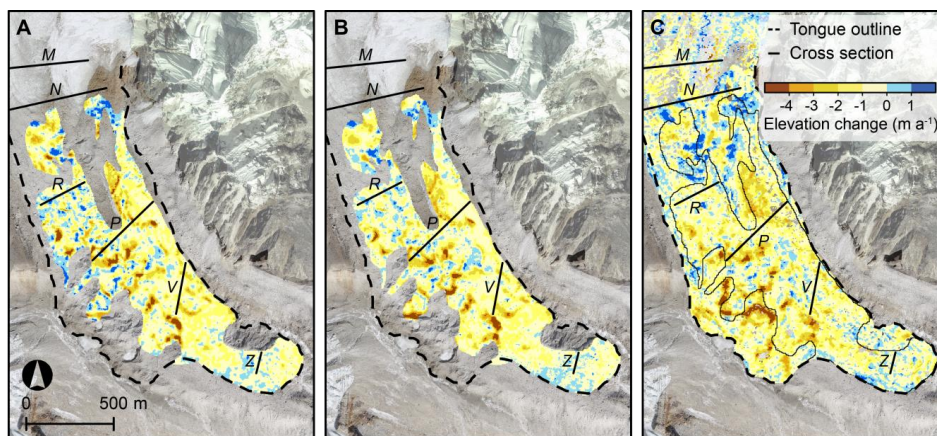
757

758 *Figure 5: Surface elevation profiles (m asl) for 2011 (black), 2014 (blue), and 2015 (red) from DGPS*
 759 *measurements (dots), terrestrial photogrammetry (black and blue lines), and UAV survey (red lines).*
 760 *Note that the right (left) bank is on the left (right) of each profile.*

761



762

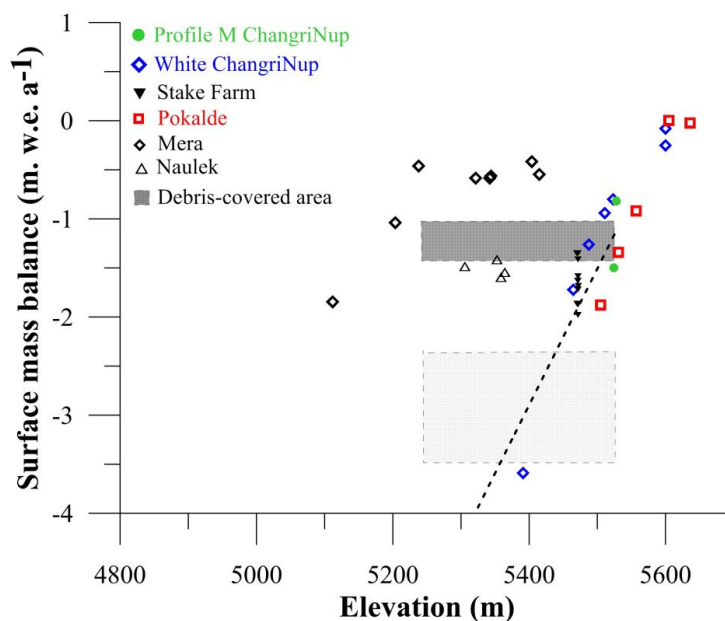


763

764 *Figure 6: Elevation changes ($m a^{-1}$) for the periods A) 2011-2014 B) 2011-2015 and C) 2009 and 2014*
765 *from photogrammetry and UAV measurements (A, B), and satellite imagery (C). The debris-covered*
766 *tongue is outlined with a dashed line.*



767



768

769 *Figure 7: Surface mass balance as a function of elevation for Changri Nup, Mera, and Pokalde glaciers*
770 *over the period 2011-2015. The grey dashed line represents the mean vertical gradient of mass balance*
771 *observed at White Changri Nup glaciers, and is extrapolated from the mean of SMB measurements at*
772 *profile M. The lower rectangle with a light grey shading corresponds to the surface mass balance of an*
773 *hypothetic clean-ice glacier. Note that surface mass balances of the stake farm on Changri Nup Glacier*
774 *were measured only in 2014-2015 only.*

775